electronics

MDPI

Article

A Variable Speed Pumped Storage System Based on Droop-Fed Vector Control Strategy for Grid Frequency and AC-Bus Voltage Stability

Girmaw Teshager Bitew [1,*], Minxiao Han [1], Sifrash Amogne Mekonnen [2] and Patrobers Simiyu [1]

[1] State Key Laboratory of Alternate Electrical Power System with Renewable Energy Sources, School of Electrical and Electronics Engineering, North China Electric Power University, Beijing 102206, China; hanminxiao@ncepu.edu.cn (M.H.); simiyupr@yahoo.com (P.S.)

[2] Social Science and Humanity College, Debre Markos University, Debre Markos 269, Ethiopia; gbitew1983@yahoo.com (S.A.M.)

* Correspondence: 1154300005@ncepu.edu.cn; Tel.: +86-155-1026-0077

Received: 7 May 2018; Accepted: 3 July 2018; Published: 7 July 2018

Abstract: Harnessing wind energy is the most rapidly growing amongst renewable energy sources. However, because of its intermittency in nature, wind power results in unfavorable influences on power system control, operation and stability. The voltage sag and flicker and grid frequency fluctuation are significant in this regard. To minimize the effect of wind power fluctuations and other contingencies on the grid frequency and AC-bus voltage, this paper presents a droop-fed vector control strategy based variable speed pumped storage (VSPS) system comprising the doubly fed induction machine. Modelling of the system is undertaken based on a phasor model technique. The case study is made by considering the droop-controlled VSPS plant in a grid containing conventional synchronous machines for hydropower and thermal power plants and an induction machine wind farm. The performance is validated and analyzed using a MATLAB/Simulink platform. The proposed droop-fed control model is compared with the conventional control strategy (without being droop-fed) and tested to wind power fluctuations, start-up transients, load variations and three-phase fault. The results show that the droop-fed vector control strategy of the VSPS plant achieves better dynamic and steady state controlling responses for grid frequency and AC-bus voltage in the power system than the conventional vector control scheme during wind power fluctuations and contingencies.

Keywords: variable speed pumped storage system; droop control; vector control; phasor model technique

1. Introduction

Due to increasing environmental concerns and energy markets, wind power generation has undergone rapid growth. In 2013, the world wind power production capacity was 318 GW and is forecasted to reach 712 GW, 1480 GW, 2089 GW and 2672 GW by 2020, 2030, 2040, and 2050, respectively, in a moderate scenario. China records the fastest growth in this regard [1,2].

Wind energy production is eco-friendly, sustainable, space efficient, incredible domestic potential, has low operational cost, revitalizing to rural economies, etc. However, the major drawback of wind power is its intermittency in nature over time, hence, significant wind power fluctuations can be observed. For a power system even with moderate wind power penetration, the fluctuations should be mitigated, otherwise this may lead to substantial deviations in the grid frequency [3], voltage sag and flicker at the grid buses [4], steady state voltage deviation, even equipment damage and system

collapse at large. A study in [5] shows that the variable speed pumped storage (VSPS) system can improve the steady state operations and dynamic stability of the power system. Having dependable features, the VSPS plant can play a key role in stabilizing the dynamics and transients of the grid affected by wind power fluctuations and other contingencies [6–11].

So far, many works have been done on the control strategies doubly fed induction machine in doubly fed induction machine (DFIM) based applications. Vector control strategy is predominantly taken into account in this regard. According to the references [8,9,12–16], the very common applicable vector control strategies implemented in DFIM are field oriented control (FOC) and direct torque control (DTC).

Based on the concept of the DTC, the direct power control (DPC) strategy is adopted. DPC is applied in an electrical machine field and has been widely studied. In DPC, the control of the real and reactive instantaneous power is independent, direct and simple [17,18]. It is noted that DPC has noble features than FOC particularly in the variable speed application [13,16,19]. Moreover, a comparative study between DPC and FOC strategies for doubly fed induction generator (DFIG) has been conducted in [19] and attempts to assure having lower computational complexity and machine model dependency, direct controllability of active and reactive powers, very good transitory response and lower overall implementation complexity than FOC. DPC is also characterized by its fast dynamic response against parameter variations and it does not utilize a rotor current control loops. In the DPC strategy, the estimations of active and reactive powers are carried out using current measurements, and directly controlled with hysteresis controllers and a switching table [12,14].

On the other hand, DPC has drawbacks compared to the FOC strategy. It has high ripples of active and reactive powers, high switching frequency which presents a high harmonic distortion of the generated currents, and provides warming-up of the silicon switchers [16]. Based on the comparative study in [16], it is hardly to state on the superiority of DPC versus FOC owing to the balance of the merits of them.

Regardless of its types, DPC or FOC, vector control confirms the higher level performance improvements in grid frequency and AC-bus voltage regulation with the implementation of the phasor model technique. However, the study of vector control in DFIM based VSPS application with the implementation of the phasor model technique is limited. The frequency regulator based on DPC implemented in a full-size converter fed synchronous machine was, for example, conducted in [8], but DFIM would be better advantages than synchronous machine in the implementation of VSPS plant for its efficiency and control [20]. The reference [13] also attempts to explore DPC in DFIG based wind power system. The DPC in [11] was also studied for the application of DFIM-based VSPS system with emphasis on converter topology study. Implementing an H-bridge cascaded multilevel converter for VSPS based on a stator voltage FOC strategy has been presented in [9] for suppressing the effect of a wind farm power fluctuations. Moreover, power filtering algorithm solution control approach was proposed in [3] to regulate the deviations of the grid frequency caused by wind power fluctuations. DPC is also studied in [11–16,19] and FOC is in [16,19] as well. The aforementioned works have not considered the phasor model simulation technique as significantly important in the large power system stability and control analysis where simulation time and computational storage are very critical. Since the electromagnetic transients are not of interest, the dynamic simulation time is highly reduced in the phasor model technique because the sinusoidal voltages and currents are replaced with phasors expressed in polar form. Implementing a phasor model in any linear system is also an advantage in that since the studies of a small-signal stability are based on eigenvalue analysis of the linearized power system, the eigenvalue analysis is complemented with dynamic simulations of the non-linear system [21,22]. Nevertheless, when implementing a phasor model technique in the DFIM application, grid frequency controlling is challenging. In the phasor model technique, the grid frequency is fixed to a constant value. It is difficult to develop a phasor locked loop which is used to synthesize the frequency. Thus, the grid frequency control is made through the active power control strategy which is

an open loop control scheme for the frequency as shown in Figure 1. As a result, the responses in the grid frequency lack dynamic performances especially during contingencies [23].

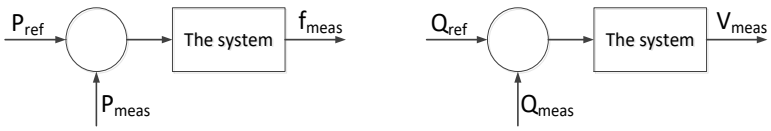

Figure 1. Open-loop frequency and AC-bus voltage control through the power control strategy.

On the other hand, the frequency has a droop characteristic with active power in the converter system. Due to the imposed frequency droop, the converter will respond to the decrement of the frequency by increasing the inverted power or by reducing the rectified power. So, the frequency droop is estimated per unit increment of rectified power to be fed to the closed control system. Since a change in the converter power results in a change in DC voltage level, a frequency decrement will be manifested as decrement in DC voltage level in an AC/DC interface system which in turn results in demanding a power flow compensation [24]. Therefore, this problem can be resolved by incorporating a synchronous machine in the power grid system helping to get the measured and estimated frequency to the VSPS control system since the rotor speed of the synchronous machine is the same as the grid frequency with a proportion factor.

Regarding voltage regulation, the AC voltage can be controlled either by reactive power control or constant voltage control. Considering the reactive power PI control, the steady state deviation of AC voltage can be observed. For a constant voltage control strategy, generating or absorbing reactive power by the VSC converter is distorted during disturbances, hence leading to significant voltage sag and flicker and steady state voltage magnitude deviations. Therefore, combining these strategies together provides droop based power control resulting in fast dynamic control response and minimized error in steady state values. Therefore, droop controllers are to be incorporated as the input of reactive power PI control (outer loop controller) of the conventional vector control strategy.

Hence, this paper presents a droop-fed vector control strategy based VSPS system for the reduction of wind power fluctuation and other contingencies impact on grid frequency and AC-bus voltage to resolve the steady state and dynamic performance problems stated in the aforementioned papers. The converter employed is the three-level neutral point clamped voltage sourced converter (NPC-VSC). Due to its novel features to the VSPS plant, the DFIM is deployed. To validate the performance of the proposed system, a phasor model simulation technique is developed and analyzed in a MATLAB/Simulink platform. The performances of the proposed system are made by comparison with the conventional method. The VSPS grid connected system consisting of hydropower and thermal power with synchronous machine and wind farm with induction generator is presented for a case study. The results show that the proposed VSPS control strategy achieves better performances in the dynamic and steady state responses of the grid frequency and AC voltage than the conventional strategy.

2. Materials and Methods

2.1. Basic Concepts of Droop Vector Control System

2.1.1. The Vector Control

Vector control is strictly defined as a variable frequency drive control method in which the stator currents of a three-phase AC electric motor are identified as two orthogonal components that can be visualized with a vector [25]. One of the two components states the torque and the other magnetic flux of the machine. From the flux and torque references, the drive control system calculates the corresponding current component references. To keep the measured current components at their reference values, typically PI controllers are used. A single-variable scalar (V/f) control will be

universally displaced by the vector control strategy due to increase of the microprocessors vector control computational power. It is applicable to both induction and synchronous machines.

The very common applicable control strategies named FOC and DTC are categorized under vector control scheme [8,16]. They are different on the operation principle but their objectives are the same. Both of them aim to control effectively the machine torque and flux, and have been successfully implemented [16]. The FOC controllers move the stator field so that it is perpendicular to the rotating rotor field. The FOC is an attractive control method but it also has a drawback. The precise knowledge of the motor parameters are, for example, mandatory. It is particularly difficult to measure precisely with a varying temperature. The DTC, which is a more robust control scheme, provides for estimating the stator flux and electric torque of the machine from terminal measurements in the stationary reference frame. The DPC strategy adopted based DTC was initially developed in 1998 [26] and implemented to DFIG in 2006 [12]. A DPC is characterized by its fast dynamic response against parameter variations and it does not utilize a rotor current control loops. The DPC also has drawbacks with high ripples of active and reactive powers, high switching frequency of which presents a high harmonic distortion of the generated currents, and provides warming-up of the silicon switchers [16].

2.1.2. The Droop Control

The main concept of droop control is to build an additional VSC-DC link frequency and AC voltage control on top of the state-of-the-art frequency and AC voltage control approach to provide virtual reserve through VSC-DC link systems. In case of the power change due to load or supply variation, the droop characteristics of grid frequency and AC voltage is observed in the VSC-DC link based system performance as is strongly related to change of power.

The frequency control structure given in Figure 2 provides a governor like droop behavior through active power loop. If there are generating units in the power system, the load sharing is determined by the frequency droop of each power generating unit, which is defined as $R = \Delta\omega/\Delta P$. For two power generating units with frequency droops R_1 and R_2, the following relationship is established for the power output ΔP_1 and ΔP_2:

$$\frac{\Delta P_1}{\Delta P_2} = \frac{R_2}{R_1} \tag{1}$$

The power generating unit with smaller frequency droop shares more loads in the power system. Accordingly, the frequency droop of the VSC-DC link with the proposed frequency controller can be expressed as

$$\Delta f = \frac{1}{K_f}(P_{ref} - P) \tag{2}$$

where K_f is the droop constant.

Likewise, if two or more alternating-voltage-controlling units are connected to a common bus in the power system, the alternating voltage controls should be coordinated to avoid hunting between the units. The transformer used in the application of VSC is to transform the grid or load bus voltage to a suitable voltage. Nevertheless, the VSC-based system performance is affected due to voltage droops of the transformer [27]. Thus, instead of controlling the alternating voltage of the point-of common-coupling (PCC), the VSC-DC link and the synchronous generator both control voltages between their own terminal/filter-bus voltages and the voltage of the PCC to give a droop characteristic to their alternating-voltage controls. So, the virtual inertia is provided through the reactive power or AC voltage control loop of the VSC system. Since the voltage is strongly related to the reactive power generation or absorption, its droop needs to be compensated via a reactive power control loop as shown Figure 2.

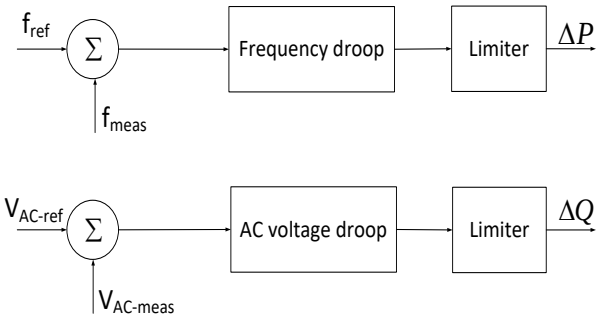

Figure 2. The block diagram of the droop control.

2.2. The Proposed System Modelling

The structure of the proposed system in this paper is illustrated in Figure 3. As shown in the figure, the DFIM of the VSPS is configured in such a way that the rotor is connected with the rotor side NPC-VSCr and the stator is connected with the grid, whereas the grid side NPC-VSCg is connected with the grid through the coupling inductor. Details are explained in [23]. The wind farm is also connected to the grid with the conventional machine. The control structure is hierarchical having inner loops (current PI controllers), outer loops (power PI controllers) and droop controllers (frequency droop controller and AC voltage droop controller).

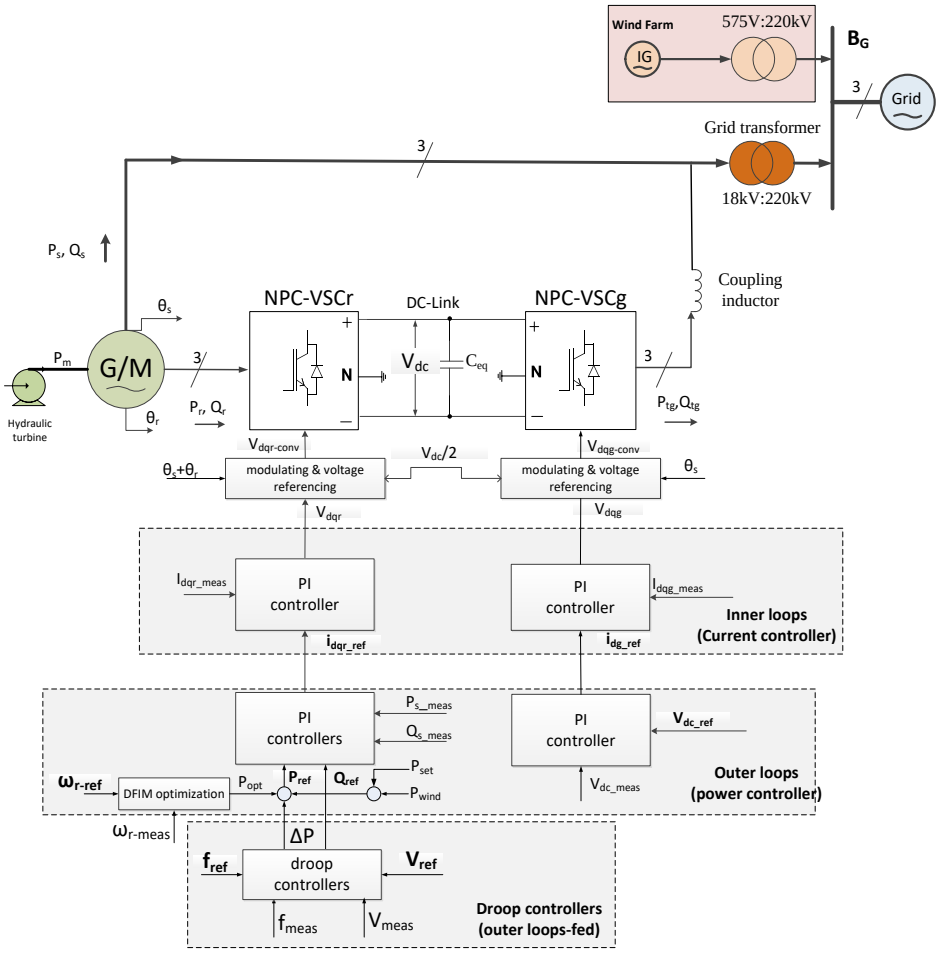

Figure 3. Structure of droop-fed vector control strategy for the NPC-VSC topology of the VSPS-wind-grid integrated system.

2.3. Machine and Converter Modelling

Detailed modelling of the hydraulic-turbine, the DFIM and the NPC-VSC is presented in [23] and the wind farm also in [15] by the same authors. This paper focuses on developing the control strategy of the VSPS in the wind-grid-integrated system for analyzing the dynamic behavior and performance of controlling the grid frequency and AC-bus voltage during the fluctuation of wind energy and other contingencies.

2.4. Control Modelling in MATLAB Platform for Dynamic and Steady State Analysis

Referring to [15,23], we have the stator power equations and the dynamics equations of the induction machine fluxes in (3) and (4) respectively.

$$\begin{aligned} P_s &= 1.5(v_{qs}i_{qs} + v_{ds}i_{ds}) \\ Q_s &= 1.5(v_{qs}i_{ds} - v_{ds}i_{qs}) \end{aligned} \tag{3}$$

$$\begin{aligned} \tfrac{d\Psi_{ds}}{dt} &= V_{ds} - R_s i_{ds} - \omega_s \Psi_{qs} \\ \tfrac{d\Psi_{qs}}{dt} &= V_{qs} - R_s i_{qs} + \omega_s \Psi_{ds} \\ \tfrac{d\Psi_{dr}}{dt} &= V_{dr} - R_r i_{dr} + (\omega_s - \omega_r)\Psi_{qr} \\ \tfrac{d\Psi_{qr}}{dt} &= V_{qr} - R_r i_{qr} - (\omega_s - \omega_r)\Psi_{dr} \end{aligned} \tag{4}$$

Based on the detail works in [23], from (3) and (4), the stator power (P_s, Q_s) is determined and expressed as a function of the rotor dq-axis current.

$$\begin{aligned} P_s &= 1.5V_s(L_m/L_s)i_{qr} \\ Q_s &= 1.5V_s[(\Psi_s/L_s) - (L_m/L_s)i_{dr}] \end{aligned} \tag{5}$$

Equation in (5) implies the independent control of the real power and reactive power in the application of a DFIM-based VSPS system, and equations in (6) have been also derived based on the assumptions taken; a voltage drop across stator resistor being very small compared to the grid voltage and a magnitude of stator flux fairly constant.

$$\begin{aligned} V_{qr} &= R_r i_{qr} + L_r^* \tfrac{di_{qr}}{dt} + (\omega_s - \omega_r)(L_r i_{dr} + L_m i_{ds}) \\ V_{dr} &= R_r i_{dr} + L_r^* \tfrac{di_{dr}}{dt} - (\omega_s - \omega_r)(L_r i_{qr} + L_m i_{qs}) \end{aligned} \tag{6}$$

where $L_r^* = L_r - (L_m^2/L_s)$ and V_{qr} and V_{dr} are feed-forward voltages to the controller.

Thus, the dynamics of the rotor dq-axes currents are controlled by developing the PI control loops from (6) which in turn are used to control the stator active power which is the function of rotor dq-axes current as equated in (5). However, dynamics of i_{dr} and i_{qr} are coupled due to the presence of the terms $L_r(\omega_s - \omega_r)$ in (6). Since the VSC controls the DFIM rotor terminal voltage, as stated in (6), i_{qr} and i_{dr} are to be related to the new control inputs u_{qr} and u_{dr}. To decouple the dynamics, the new control inputs are introduced and is redefined as in (7).

$$\begin{aligned} u_{qr} &= V_{qr} - (\omega_s - \omega_r)(L_r i_{dr} + L_m i_{ds}) \\ u_{dr} &= V_{dr} + (\omega_s - \omega_r)(L_r i_{qr} + L_m i_{qs}) \\ \text{where } u_{dr} &= L_r^* \tfrac{di_{dr}}{dt} + R_r i_{dr} \\ u_{qr} &= L_r^* \tfrac{di_{qr}}{dt} + R_r i_{qr} \end{aligned} \tag{7}$$

On the other hand, in the grid side of NPC-VSCg converter, the PI control of DC voltage in the DC link is deployed for regulating the proper active power exchange between the converter and the grid on the outer loop whereas PI current controller is used on the inner loop. But, reactive power

exchange is usually set to zero [28]. The mathematical model design is made by the equation in (5) denoting the voltage equations across the coupling inductor.

$$\begin{aligned} V_{dg} &= R\mathrm{i}_{dg} + L\frac{di_{dg}}{dt} - \omega_s L i_{qg} + V_{ds} \\ V_{qg} &= R\mathrm{i}_{qg} + L\frac{di_{qg}}{dt} + \omega_s L i_{dg} + V_{qs} \end{aligned} \tag{8}$$

where R and L are the coupling inductor resistance and inductance respectively; and V_{dqg} and V_{dqs} are control inputs and disturbance inputs respectively.

Similarly, i_{qg} and i_{dg} are to be related to the new control inputs u_{qg} and u_{dg} and (9) is redefined as

$$\begin{aligned} u_{dg} &= V_{dg} + \omega_s L i_{qg} - V_{ds} \\ u_{qg} &= V_{qg} - \omega_s L i_{dg} - V_{qs} \\ \text{where } u_{dg} &= L\frac{di_{dg}}{dt} + R i_{dg} \\ u_{qg} &= L\frac{di_{qg}}{dt} + R i_{qg} \end{aligned} \tag{9}$$

Thus, from (7) and (9), the rotor and grid current control loops (inner loops) are developed. Both current controllers are supported by feed forward terms predicting V_{dqr} and V_{dqg}. The dynamics of the DC voltage in the DC link is defined by (10). The converters and DC-link are assumed to be lossless.

$$\frac{dV_{dc}}{dt} = \frac{1}{C} i_{dc} = \frac{1}{CV_{dc}} (\mathrm{P}_r - \mathrm{P}_g) \tag{10}$$

where C and V_{dc} are the DC link capacitance and DC voltage respectively. P_g and P_r are active power flow in the grid and rotor side of the converters respectively.

The power equations of (3) also hold for a grid side power flow and denoted by (11).

$$\begin{aligned} P_{tg} &= 1.5(v_{qg} i_{qg} + v_{dg} i_{dg}) \\ Q_{tg} &= 1.5(v_{qg} i_{dg} - v_{dg} i_{qg}) \end{aligned} \tag{11}$$

2.5. Control of Active and Reactive Power for Rotor Side Converter

Active or reactive power is controlled by the rotor side converter which connects rotor windings and DC link. This converter offers a proper AC excitation for the windings of the rotor that provides the stator windings proper active power.

2.5.1. Active Power Control

Controlling of active power can ensure controlling of system frequency. So as to keep the grid frequency constant, synchronous generators, for example, can have a permanent droop control loop in the turbine control. It is dedicated to adjust the active power balance between the production and the consumption of the system. On the other hand, implementing the primary frequency control in the DFIM-based VSPS unit, which is critically important, controls the active power flow of the system. In this application, a vector control strategy is employed to have fast dynamic response and lets the control system compensate effectively during contingencies. Even if this is a limited control scheme that is placed in the VSPS unit, the significant output that is an adjustable and nearly constant power flow can be seen from the network of the power system as far as the VSPS operates within the specified limits. The power command P_{opt} of the control system of the VSPS is determined from the capacity of the VSPS unit and its efficiency. An external set point, P_{set} which is the input to the power control system, in this regard, should be assumed for the VSPS. The set point depends on the VSPS capacity and the situation of the power grid. The value of this set point is dedicated to optimize the system energy balance and update relatively with slow rate. The main concern is, however, to control the contingencies and regulate the VSPS power for mitigating the impact on the grid stability.

As illustrated in Figure 3, the rotor-side converter control is modelled in two stages. The first stage is power (PQ) control (the outer loop) in that the active/reactive power tracks the respective reference. This loop provides dq-axis reference currents for the second stage (the inner loop). The inner loop is technically a current control offering dq-axis reference voltage for modulation and injected to the converter. PI controllers with limiters are applied in both control stages.

The model design of the active power control of the rotor side converter is presented as follows. Referring to the voltage equations in (4), we have the mathematical equations of (6). From (6), the rotor electrical dynamics model is determined based on the system equations and representing two decoupled, first-order subsystems. It can control i_{dqr} by u_{dqr}, in turn, u_{dqr} can be delivered by corresponding PI compensators. The compensators process the current errors and provides u_{dqr}. The control plants in dq-axis current-control loops are identical. Therefore, the corresponding compensators can also be identical. Thus, the compensator can be a simple proportional-integral (PI) compensator, $K_i(s)$ to enable tracking of a respective reference. The compensator is defined by

$$K_i(s) = \frac{P_i s + I_i}{s} \tag{12}$$

Thus, the loop gain becomes

$$\ell(s) = \left(\frac{P_i}{L_r^*}\right)\frac{s + I_i/P_i}{s + R_r/L_r^*} \tag{13}$$

Due to the plant pole at s = $-R_r/L_r$*, which is fairly close to the origin, the magnitude and the phase of the loop gain start to drop from a relatively low frequency. Thus, the plant pole is first canceled by the compensator zero s = $-I_i/P_i$, and the loop gain assumes the form $\ell = P_i/L_r^*$. Then, based on the plant function, $G_i(s) = 1/(L_r^* s + R_r)$ developed from (7) and considering the compensator $K_i(s)$ in, the closed-loop transfer function becomes;

$$\frac{I_{dqr}(s)}{I_{dqr-ref}(s)} = G_{ic}(s) \approx \frac{1}{\tau^* s + 1} \text{ if } P_i = L_r^*/\tau^* \text{ and } I_i = R_r/\tau^* \tag{14}$$

where P_i and I_i are proportional and integral gains and $\tau^* = L_r^*/R_r$. The gains are determined and tuned based on the control stability theory. The control structure of the inner loop is illustrated in Figure 5a.

From Equation (14), the q-axis rotor current as a function of its own reference value is obtained.

$$I_{qr}(s) = G_{ic}(s) I_{qr-ref}(s) \tag{15}$$

Multiplying both sides of (15) by 1.5 VsLm/Ls, we get

$$1.5 V_s L_m / L_s I_{qr}(s) = G_{ic}(s) 1.5 V_s L_m / L_s I_{qr-ref}(s) \tag{16}$$

Therefore, based on Equation (5), from (16), we can deduce (17).

$$P_s(s) = G_p(s) P_{s-ref}(s) \tag{17}$$

From these relationship, we can have the block diagram of Figure 4.

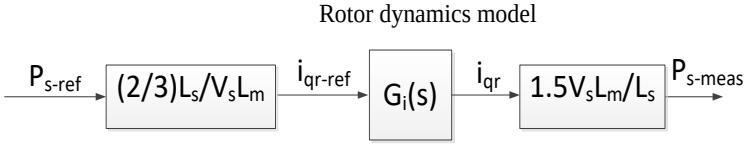

Figure 4. Control block diagram of the vector controlled DFIM for active power control loop.

Thus, plant function $G_p(s)$ is defined by multiplying $G_{ic}(s)$ with 1.5 VsLm/Ls i.e., $G_p(s) = 1.5V_sL_m/L_s(L_r^*s + R_r)$. Accordingly, the closed loop active power control is developed as shown in Figure 5b. The PI control of $K_p(s)$ of Figure 5b processes the error signal e_p and provides the reference current $i_{qr\text{-}ref}$ and defined by;

$$K_p(s) = \frac{P_p s + I_p}{s} \tag{18}$$

where P_p and I_p are proportional and integral gains. The open loop transfer function becomes;

$$G_{po}(s) = \left(K\frac{(P_p s + P_i)(I_p s + I_i)}{L_r^* s^3 + (R_r + I_p)s^2 + I_i s}\right) \tag{19}$$

where K = 1.5 VsLm/Ls. We used the symmetrical optimum method to determine the control gains (P_p and I_p) since the open loop transfer function has a pole at the origin. This method optimizes the system's control behavior. Thus, the inner current loop with wider bandwidth of 2.4 Hz than the outer power loop with 1.11 Hz is designed.

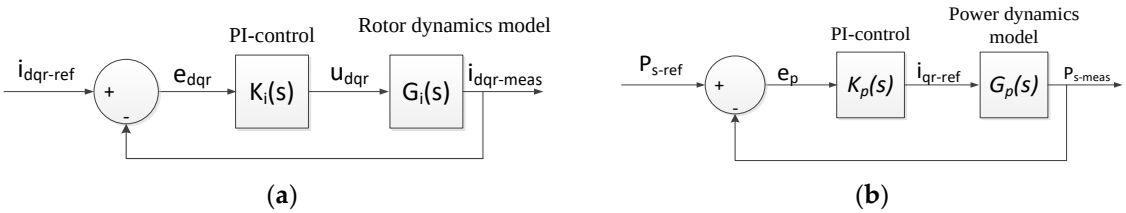

Figure 5. The PI control structure of the NPC-VSCr: (**a**) the current controller (inner loop); (**b**) the active power control (outer loop).

Permanent droop should be included in this control as active power in DFIM is controlled by the converter. In dominant wind farm power production fluctuations, the response of the power system to contingencies is highly improved if a frequency droop control scheme is included in the active power control loop. The power transfer within the DC-link can be modulated by a frequency droop control. It can be modelled as an additional signal that is added to the active power reference P_{ref} in Figure 6.

According to Figure 6, the difference between actual and reference frequency is forwarded to a proportional controller which defines permanent droop. The proportional output is added to the signal of the active power P_{set} and the optimized output power P_{opt} from the induction machine and the sum of them presents the active power reference P_{ref} for the PI active power control in the outer loop.

The optimized power P_{opt} is the very beginning reference power of the VSPS control system which is determined by considering the capacity of the hydraulic turbines of the VSPS plant along with its losses. Since the plant is a variable speed scheme, the control system enables to adjust and regulate the plant when the power variation occurs in the grid. Thus, we can add the power command $\Delta P_{wind} = P_{wind} - P_{set}$ to the VSPS power control unit and to be compensated. P_{wind} is the wind farm power measured which is subject to the fluctuation due to its intermittency. Then, it is designed for the converters to offer frequency support to the grid. This control structure provides a governor-like droop behavior through active power flow. The droop-type control is built based on the concept of power synchronization control in which grid synchronization is achieved regardless of a dedicated synchronization unit [21]. This droop-type control system provides a DC link with frequency droop characteristic. For other power generating units in the grid system, the load sharing is possible.

Hence, with the additional power command ΔP_f due to change of frequency caused by all contingencies to the VSPS active power control system, improvement of the dynamics performance of the power system can be ensured, and (20) is accordingly determined.

$$\Delta P_f = K_f(f_{ref} - f_{grid}) \tag{20}$$

where K_f is the droop constant, f_{ref} is the reference frequency in which 50 Hz applied in this paper, and f_{grid} is the grid frequency measured and estimated from the rotor speed of the synchronous machine in the same grid.

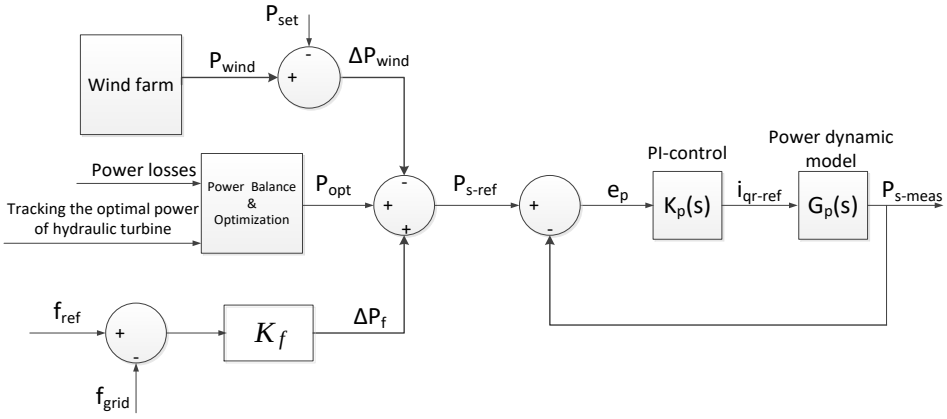

Figure 6. A rotor-side converter of active power control structure.

2.5.2. Reactive Power Control

The same procedures following as in the active power modelling section, the reactive power control system is developed. From the Equations (5), (14) and Figure 5, the model (21) is determined.

$$Q_s(s) = G_q(s)Q_{s-ref}(s) \tag{21}$$

Hence, the dynamic model for the reactive power control of rotor side converter VSC-NPCr is developed, and the PI control of $K_q(s)$ is defined in (22).

$$K_q(s) = \frac{P_q s + I_q}{s} \tag{22}$$

The rotor side converter provides the proper reactive power of stator windings as stated above. Therefore, in order to keep the AC-bus voltage constant, i.e., to adjust the generation and absorption of the reactive power in the converter, additional signal should be included to the reference reactive power. With load compensation, referring Figure 7, for parallel connected voltage control units, the magnitudes of the resulting compensated voltages can be given by

$$\begin{aligned} V_{t-SG} &= e_{SG} + k_{SG}(\mathrm{R}_{SG} + \mathrm{jX}_{SG})\mathrm{i}_{SG} \\ V_{t-vsc} &= e_{vsc} + k_{vsc}(\mathrm{R}_{vsc} + \mathrm{jX}_{vsc})\mathrm{i}_{vsc} \end{aligned} \tag{23}$$

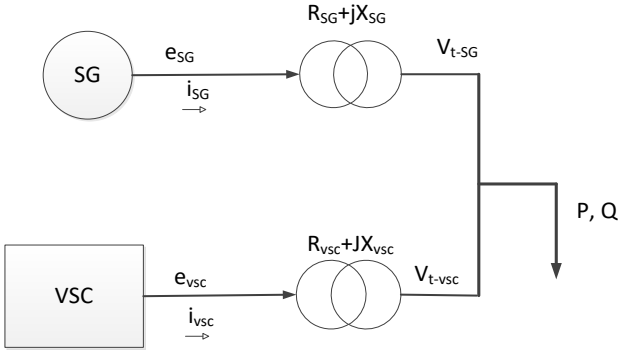

Figure 7. Voltage droop control for parallel connected voltage-control units.

In order to provide appropriate AC voltage in the network, for example, the DFIM reactive power can be properly controlled. This control can be accomplished based on the control structure presented in Figure 8. This figure indicates that the difference between actual AC voltage V_{meas} and reference AC voltage V_{ref} of the AC grid is integrated and added to the reactive power set signal Q_{set} and the sum of both signals presents the reference of the reactive power Q_{ref} for the PI reactive power control on the outer loop of the VSPS control system provided in the rotor side.

From (23), the voltage-reactive power relationship of Equation (24) with the droop constant K_{ac} is derived.

$$\Delta Q_{vsc} = K_{ac}(V_{ref} - V_{meas}) \tag{24}$$

The voltage control structure through the reactive power control loop is illustrated in Figure 8.

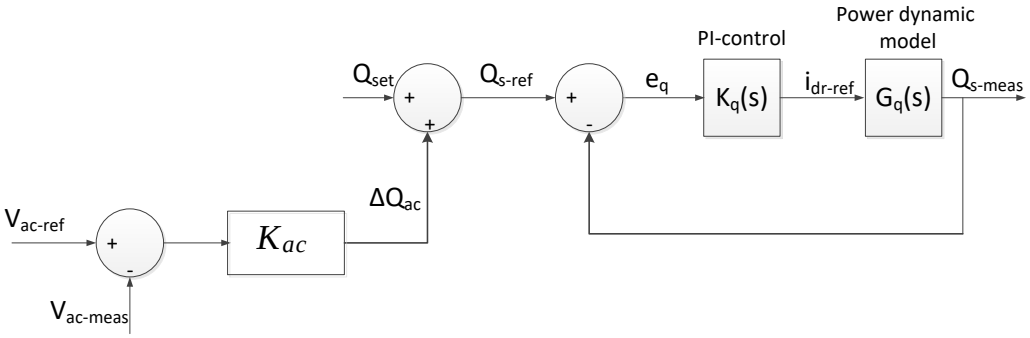

Figure 8. A rotor-side converter of reactive power control structure.

2.6. Control of Active and Reactive Power for Grid Side Converter

The reactive power on the grid side converter is controlled by a PI controller by setting its reference value zero. Whereas the proper active power exchange between the converter and grid is controlled through the PI control of DC voltage in the DC link.

For control design purposes, the d-axis is supposed to be set in phase with the voltage across the resistor. Thus, the d-component of the voltages in d-q coordinates becomes v_{dg} and zero that of v_{qg}. So, the power equations of (11) is deduced by (25).

$$\begin{aligned} P_{tg} &= 1.5 v_{dg} i_{dg} \\ Q_{tg} &= -1.5 v_{dg} i_{qg} \end{aligned} \tag{25}$$

Ignoring the losses and harmonics due to switching in the converter, the real power balance equation on the grid side can be given by:

$$P_{tg} = 1.5 v_{dg} i_{dg} = V_{dc} I_{dc} \tag{26}$$

Equation (26) implies that the DC-bus voltage is likely and independently controlled by controlling the d-axis current i_{dg}.

The objective of the active/reactive power controller of the VSC system is to regulate the active/reactive power exchange between the converter and the AC grid. In this controller, for the sake of mathematical formulation, it is supposed to be the DC side of the VSC is connected to an ideal DC voltage source that dictates the DC-bus voltage as shown in Figure 9.

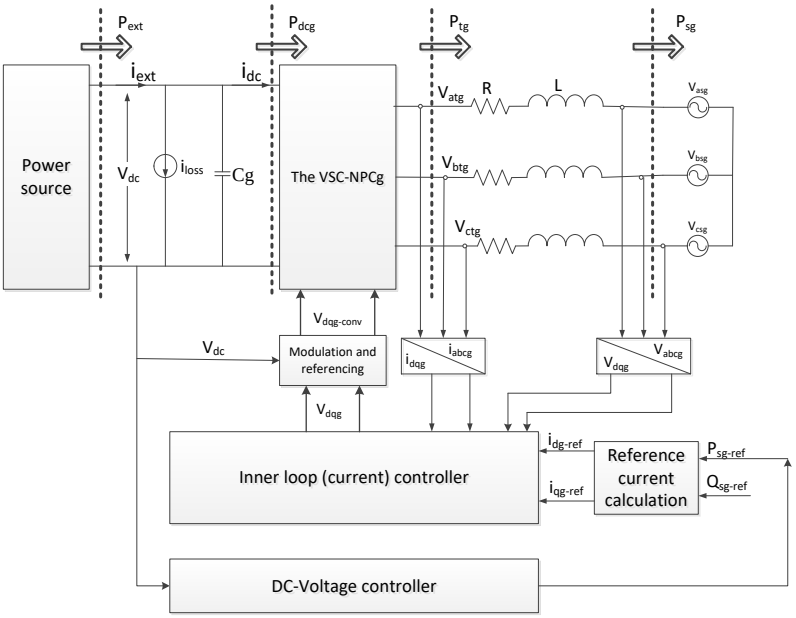

Figure 9. Simplified schematic diagram of the controlled DC-voltage power port of a three-level NPC-VSCg.

According to Figure 9, any power imbalance within the outlined area results in excursions (and potential instability) of the DC-bus voltage since there is no DC voltage source in the VSC system. Thus, the DC-voltage V_{dc} of the grid port requires proper regulation. $P_{ext}(t)$ cannot be controlled by the VSC system since it is typically an exogenous signal. Thus, to ensure the power balance exchange, P_{dcg} must be controlled through the VSC system. Based on Figure 9, the power balance is expressed by (27).

$$P_{ext} - V_{dc}i_{loss} - \frac{d}{dt}(\frac{1}{2}C_g V_{dc}^2) = P_{dcg} = V_{dc}i_{dc} \tag{27}$$

However, for a three-level NPC-VSC, the DC bus effective capacitance is half each of its DC-side capacitors. Ignoring the power losses related to the IGBT resistance r_{on} and substituting for $P_{dcg} = P_{tg}$ and rearranging the resultant, (27) is rewritten as (28).

$$P_{ext} - \underbrace{V_{dc}i_{loss}}_{P_{loss}} - \frac{d}{dt}(\frac{1}{2}C_g V_{dc}^2) = P_{tg} \tag{28}$$

where P_{tg} is the power at the AC-side terminal of the VSC. Equation (28) represents a power balance and describes a dynamic behavior of V_{dc} of a system in which V_{dc}^2 is the output state variable, the P_{tg} is the control input, and P_{ext} and P_{loss} are the exogenous inputs. C_g is the capacitance for smoothing the DC-bus voltage ripples.

Similarly, taking into account the system on the rotor side converter encompassing C_r, the following equation holds.

$$\frac{d}{dt}(\frac{1}{2}C_r V_{dc}^2) = P_{dcr} - \underbrace{V_{dc}i_{lossr}}_{P_{lossr}} - P_{ext} \tag{29}$$

Ignoring the power losses related to the IGBT resistance r_{on}, AC-side terminal power is equal to the machine rotor power $P_r = P_{dcr}$. Adding (28) and (29) together, the Equation (30) is found.

$$\frac{d}{dt}(\frac{1}{2}C_{eq} V_{dc}^2) = -P_{tg} - P_{loss} + P_{dcr} \tag{30}$$

Equation (30) describes a power-balance dynamic equation for the capacitance $C_{eq} = C_r + C_g$, which is subjected to the (relatively small) discharging power $P_{loss} = V_{dc}\,(i_{lossr} + i_{lossg})$ the (widely variable) charging power P_{dcr}, and the (controllable) discharging power P_{tg}.

Starting with the voltage equation across the coupling inductor from Figure 6, we have

$$L\frac{di}{dt} = -Ri + V_{tg} - V_{sg} \tag{31}$$

The control input P_{tg} is expressed in terms of P_{sg} and Q_{sg} since the VSC system of Figure 9 enables to control P_{sg} and Q_{sg}. Multiplying both sides of (31) by $(3/2)i^*$ (i^* is the conjugate of i), we obtain

$$\frac{3L}{2}\mathrm{Re}\{\frac{di}{dt}i^*\} = -\frac{3}{2}R\hat{i}^2 + \frac{3}{2}\mathrm{Re}\{V_{tg}i^*\} - \frac{3}{2}\mathrm{Re}\{V_{sg}i^*\} \tag{32}$$

Rearranging and solving (30) for $P_{tg} = (3/2)\mathrm{Re}\{V_{tg}i^*\}$ and $P_{sg} = (3/2)\mathrm{Re}\{V_{sg}i^*\}$, we get

$$P_{tg} = P_{sg} + \frac{3}{2}R\hat{i}^2 + \frac{3L}{2}\mathrm{Re}\{\frac{di}{dt}i^*\} \text{ or } P_{tg} = P_{sg} + \frac{3}{2}R\hat{i}^2 + \frac{3L}{4}\frac{d\hat{i}^2}{dt} \tag{33}$$

Practically, R is a small resistance and its absorbed power is negligible compared to P_{tg} and P_{sg}. However, during transients, the power absorbed by the coupling inductor can be significant. So, L must be adequately large to suppress the switching harmonics. Furthermore, since the current controllers in dq-axis frame are fast, i can undergo rapid phase and amplitude changes, during the real/reactive-power command tracking process.

From the power equation, we have

$$P_{sg} + jQ_{sg} = \frac{3}{2}(V_{sg}i^*) \text{ or } P_{sg}^2 + Q_{sg}^2 = \frac{9}{4}\hat{V}_{sg}^2\hat{i}^2 \tag{34}$$

Solving (34) for $\hat{i}^2$ and substituting in (33), Equation (35) is derived

$$P_{tg} \approx P_{sg} + \left(\frac{2L}{3\hat{V}_{sg}^2}\right)P_{sg}\frac{dP_{sg}}{dt} + \left(\frac{2L}{3\hat{V}_{sg}^2}\right)Q_{sg}\frac{dQ_{sg}}{dt} \tag{35}$$

Substituting (35) in (30), Equation (36) holds.

$$\frac{d\mathrm{V}_{dc}^2}{dt} = \frac{2}{C_{eq}}\left[-P_{loss} + P_{dcr} - P_{sg} - \left(\left(\frac{2L}{3\hat{V}_{sg}^2}\right)P_{sg}\frac{dP_{sg}}{dt} + \left(\frac{2L}{3\hat{V}_{sg}^2}\right)Q_{sg}\frac{dQ_{sg}}{dt}\right)\right] \tag{36}$$

Equation (36) describes the dynamics of V_{dc}^2; P_{sg} is the control input, Q_{sg} are the disturbance inputs. Thus, to control V_{dc}^2, one can form the control scheme shown in Figure 8, which consists of an inner control loop nested inside an outer loop. The outer loop compares V_{dc}^2 with its reference value, processes the error by a compensator, and delivers $P_{sg\text{-}ref}$ to the inner control loop. The inner control loop is basically the current controller which regulates its reference value calculated from the $P_{sg\text{-}ref}$ of the outer loop controller.

Since the control plant is nonlinear, Equation (36) should be linearized about the steady state real power flow operating points based on [29], and thus, designing $G_{dc}(s)$ accordingly. So, $P_{sg0} = P_{ext} - P_{loss} \approx P_{ext0}$; and (36) is linearized as

$$\frac{d\tilde{\mathrm{V}}_{dc}^2}{dt} = \frac{2}{C_{eq}}\left[-\tilde{P}_{ext} - \tilde{P}_{sg} - \left\{\left(\frac{2L}{3\hat{V}_{sg}^2}\right)P_{sg0}\frac{d\tilde{P}_{sg}}{dt} + \left(\frac{2L}{3\hat{V}_{sg}^2}\right)Q_{sg0}\frac{d\tilde{Q}_{sg}}{dt}\right\}\right] \tag{37}$$

where ~denotes small-signal perturbations. The time domain of (37) is transformed into Laplace domain resulting in a control plant transfer function as

$$G_{dc}(s) = \frac{\widetilde{V}_{dc}^2}{\widetilde{P}_{sg}} = -\left(\frac{2}{C_{eq}}\right)\frac{\tau s + 1}{s} \tag{38}$$

where τ is the time constant defined by

$$\tau = \frac{2LP_{sg0}}{3\hat{V}_{sg}^2} \tag{39}$$

where L, P_{sg0} and $\hat{V}_{sg}$ are respectively the coupling inductance, (steady-state) real power flow and grid-side AC voltage magnitude.

As per Equation (39), if P_{ext0} is small, τ is insignificant and the plant is predominantly an integrator since τ is proportional to the real-power flow P_{ext0} (or P_{sg0}). τ brings a phase shift in $G_{dc}(s)$ when P_{ext0} increases. In the inverting operation mode where P_{ext0} is positive, τ is positive and adds to the phase of $G_{dc}(s)$. However, in the rectifying operation mode where P_{ext0} is negative, τ is negative and reduces the phase of $G_{dc}(s)$; a larger absolute value of P_{ext0} results in a smaller phase of $G_{dc}(s)$. Based on (38), the plant zero is $z = -1/\tau$. Therefore, a negative τ corresponds to a zero on the right-half plane, and the controlled DC-voltage VSPS represents a non-minimum-phase system in the rectifying operation mode. Thus, the phase reduction associated with the non-minimum-phase zero has a detrimental impact on the closed-loop stability.

Taking into account of system model linearization, the PI controller parameters are chosen around the operating points. For the model linearization, the point of a reference is obtained by specifying a reference input V_{dc-ref}. The control structure is depicted in Figure 10a.

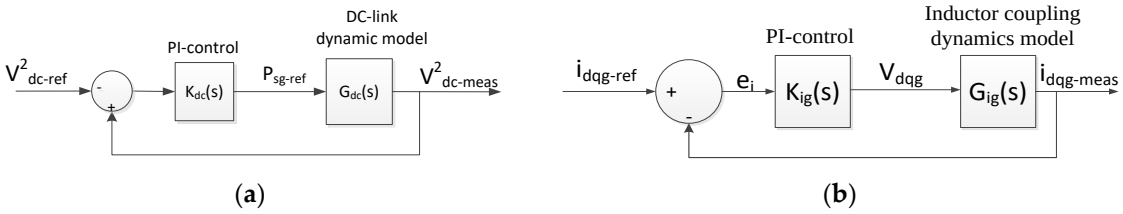

(**a**) (**b**)

Figure 10. The control structure for grid side converter of NPC-VSC: (**a**) the DC-bus voltage control (outer loop) structure; (**b**) the current control (inner loop) structure.

The compensator $K_{dc}(s)$ is designed to guarantee an adequate stability margin even if the steady state operating point changes. It is designed based on the plant function of (36) in which V_{dc}^2 is impacted by P_{ext} and P_{loss} under the steady state and transient conditions. The feed-forward compensation can reduce the impact of P_{ext}. However, the feed-forward compensation is hardly effective to mitigate the impact of P_{loss} due to uncertainty of the measurement and estimation of P_{loss}. Therefore, $K_{dc}(s)$ must have an integral term (I_{dc}) to eliminate the steady state error of V_{dc}^2 caused by P_{loss}. Because of a presence of an integral term in the control plant and to ensure an adequate phase margin and stability, a proportional term (P_{dc}) must be included in the $K_{dc}(s)$. Hence, the PI compensation $K_{dc}(s)$ of Figure 9a is defined by (40).

$$K_{dc}(s) = \frac{P_{dc}s + I_{dc}}{s} \tag{40}$$

where P_{dc} and I_{dc} are respectively proportional and integral constants of the PI controller.

The control of the inner loops in the grid side converter is designed based on the voltage dynamics equation of (8) by following the same procedure as of the rotor side. The inner loop current controllers which are identical due to identical dynamic model are dedicated to control both active and reactive

power i_{dg} for active power and i_{qg} for reactive power. Hence, PI control structure of the inner loops shown in Figure 10b is developed.

The PI controller compensation $K_{ig}(s)$ and the inductor coupling dynamic model $G_{ig}(s)$ of Figure 9b are derived and given by (41) and (42) respectively.

$$K_{ig}(s) = \frac{P_{ig}s + I_{ig}}{s} \tag{41}$$

$$G_{ig}(s) = \frac{1}{\tau s + 1}; \tau = L/R \tag{42}$$

where P_{ig}, I_{ig}; L and R respectively proportional and integral constants; inductance and resistance of the coupling inductor.

2.7. Measuring and Estimation of the Grid Frequency

The grid frequency can be detected or measured through a phase-locked loop (PLL) which is a nonlinear feedback system that generates an output signal whose phase is related to the phase of an input signal. A basic advantage of PLL is to synthesize the grid frequency in a power system.

In a phasor model, however, the PLL is ignored. In this method, the sinusoidal voltages and currents are replaced by phasor quantities (complex numbers) at the system nominal frequency (50 Hz). As a result, measuring of a frequency for controlling is, in a phasor model technique, critically challenging. As stated above, frequency is regulated in an open loop way through the active power control system and, in turn. the dynamic stability of the frequency during contingencies is not ensured. Therefore, a method to synthesize the frequency is proposed in this paper and presented as follows.

In the basic operation principle of a synchronous machine, the rotating magnetic field of the stator is synchronously moving with the speed of the rotor. The frequency of the power system in which the synchronous machine connected to is the number of cycles per second in an alternating current sine wave of the rotating magnetic field of the stator. Its value is practically 50 Hz or 60 Hz. The frequency and the rotor speed are linearly related in the synchronous machine. It is given as

$$f = \frac{p}{120}n \tag{43}$$

where f, p and n are respectively electrical frequency in Hz, number of poles and rotor speed of the machine in rpm

From (43), it is deduced that the per-unit (pu) values of the frequency and rotor speed are equal, i.e., $f_{pu} = n_{pu}$. Thus, taking the pu values of the rotor speed as the pu values of the frequency is practically acceptable. Therefore, the rotor speed is measured and estimated from the synchronous machine and synthesized into the input of the frequency droop controller of the VSPS plant which contains the doubly fed induction machine.

2.8. Voltage Modulation and Converter Reference Voltage

The self-commutated VSC converter is a fast and controllable converter for AC/DC interface applications. One type of VSC converters is a three-level NPC power converter which contains three arms with each four switching components with antiparallel diodes and two NPC diodes. Since this paper is engaged to validate the performance of the proposed system in accordance with the phasor model technique, the following assumptions are taken: the power losses in the converters are neglected and the switching dynamics can be also neglected because the frequency of a pulse width modulation in NPC-VSC is much greater than the frequency of the grid [30]. Hence, modulated and converter reference voltages of the VSCs in this paper are denoted by the equivalent phasor model equations and obtained accordingly.

The modulated voltages of the rotor-side converter are given in (44).

$$m_{dqr} = \left|(2/\mathrm{V}_{dc})\mathrm{V}_{dqr-ref} * V_{nom}\sqrt{2/3}\right| \tag{44}$$

where V_{dqr_ref}* is the feed-forward voltage in pu value and V_{nom} is the RMS nominal voltage of the VSPS plant. The converter control voltage is defined by

$$V_{dqr-cont} = \left|m_{dqr}\right|\angle(\theta_s + \theta_r + \angle V_{dqr}) \tag{45}$$

where $\angle V_{dqr}$ is an angle obtained from the feed forward voltages.

Similarly, for grid side converter, the modulated and the converter control voltages are obtained and given by the following equations.

$$\begin{aligned} m_{dqg} &= \left|(2/V_{dc})V_{dqg-ref} * V_{nom}\sqrt{2/3}\right| \\ V_{dqr-cont} &= \left|m_{dqg}\right|\angle(\theta_s + \angle V_{dqg}) \end{aligned} \tag{46}$$

where V_{dqg_ref}* is the feed-forward voltage in pu value and $\angle V_{dqg}$ is an angle obtained from the feed forward voltages.

Since the converters reference voltage should be fed in actual value, they are determined by

$$\begin{aligned} V_{dqr-conv} &= (1/2)\sqrt{3/2}(V_{dc}/V_{nom})V_{dqr-cont} \\ V_{dqg-conv} &= (1/2)\sqrt{3/2}(V_{dc}/V_{nom})V_{dqg-cont} \end{aligned} \tag{47}$$

where $V_{dqr\text{-}conv}$ and $V_{dqg\text{-}conv}$ are rotor side and grid side converter reference voltages respectively.

2.9. Case Study and Simulation Model

In this paper, a case-study is undertaken involving a 300 MW DFIM-based VSPS and a power grid system integrated with a wind-farm comprising of seven identical 15 MW wind turbine induction generators. To investigate the impact of wind fluctuations on the grid frequency, a medium power system model consisting of two 200 MVA hydropower plants and one 15 MVA diesel power unit with conventional synchronous generators is established. The phasor model technique in a MATLAB/Simulink platform is applied. For the conventional synchronous machines, the primary voltage regulation method in automatic voltage regulators based on the standard IEEE type I and the primary frequency regulation in turbine governors are used. The simulation network model setup is illustrated in Figure 11 with a single-line diagram.

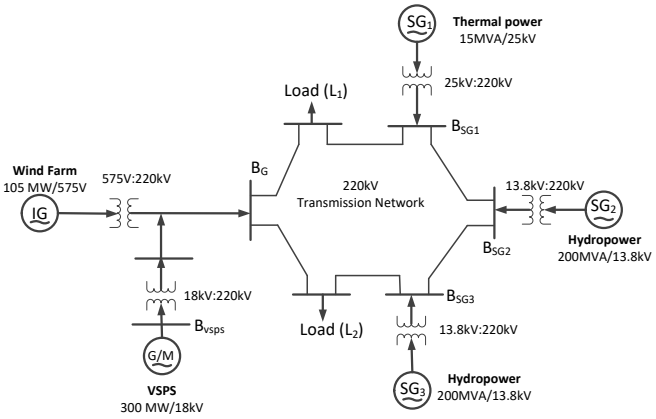

Figure 11. Single-line diagram setup of the VSPS-wind farm-grid integrated system for the case study [15].

3. Results and Discussions

The control of power in the DFIM based VSPS system is essentially the power control of the VSC fed VSPS system. The results presented in this section demonstrate the dynamics and steady-state

responses of grid frequency and AC-bus voltage control. The performances are made by comparing between the control system with and without the droop control.

3.1. VSPS Grid-Integrated Network Simulation and Implications for Regulating Grid Frequency and AC-Bus Voltage in Case of Contingencies

The control of power in the DFIM-based VSPS system with a wind farm is essentially the power control of the VSC-fed VSPS system. Figure 12 shows the evolution of the VSPS unit in the proposed network depicted in Figure 11 but excluding the wind farm and with the absence of contingencies. Generally, the reference reactive power is set to zero for a system without droop control over any operating conditions since there is no reactive power exchange between the converter and the grid. However, to show the performance of the control system, the varying active and reactive power instructional signals are given to the control system as a reference value. As shown in Figure 12a, the proposed control system tracks the power fluctuation instructions very well. A small distortion is observed while the instruction signals vary from one value to the other. A 20% overshoot is perceived during the instruction signal switches from lower to higher values. The overshoots in active power have some impact on frequency deviations. The variations in instructional signal of reactive power cause the AC voltage to deviate from its nominal value. The excursions are quickly regulated. Figure 11b shows the response of the inner loop signals when the power fluctuation instructions are imposed on the outer loop system. The response shows perfect tracking of the respective reference signals. Similarly, precise tracking of inner loop control reference signals in the droop and without droop-fed vector control of the VSPS system along with the wind power farm is also shown in Figure 13. But since the droop-fed matters to change the reference values in the dq-rotor currents, the responses between the control system with and without droop-fed in the dq-rotor currents vary. Hence, the results from Figures 12 and 13 imply that the droop-fed vector control strategy based VSPS system can adjust the grid frequency and AC voltage fluctuations caused by wind energy or other contingencies in a power grid integrated system quickly and flexibly. This is verified in the following sections.

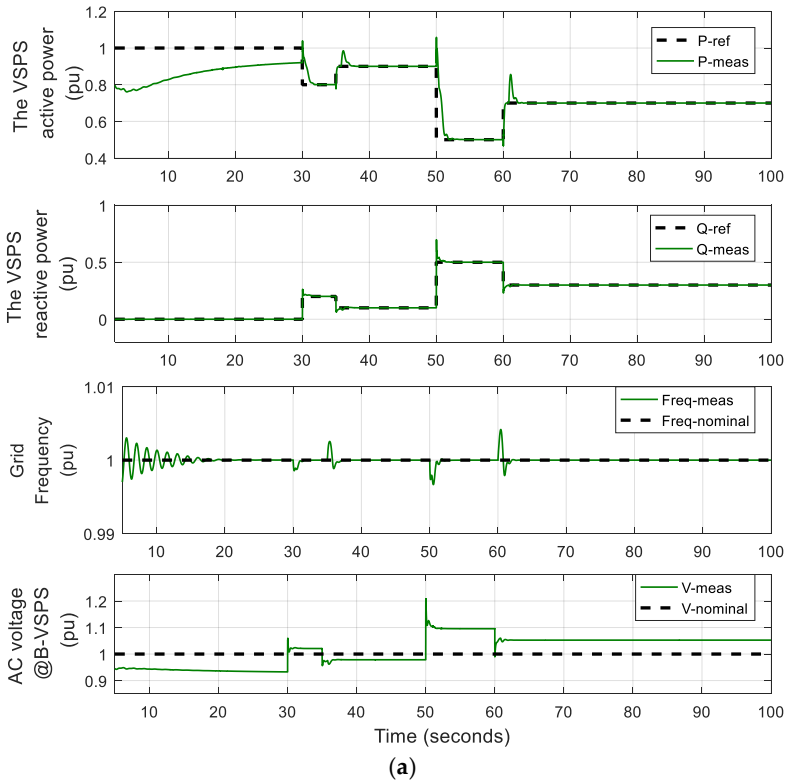

(**a**)

Figure 12. *Cont.*

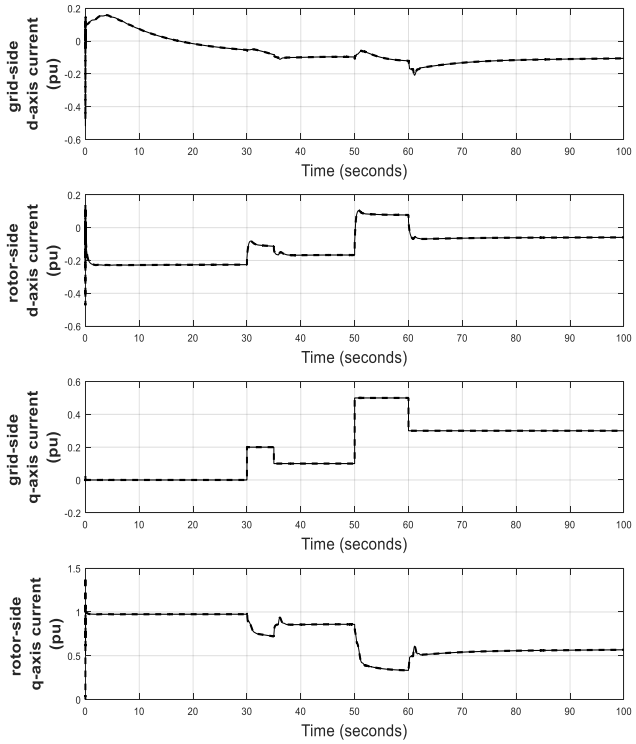

(**b**)

Figure 12. The droop-fed vector control based VSPS system without wind farm: (**a**) tracking of power instructions on outer loop control; (**b**) tracking of inner loop control reference signals.

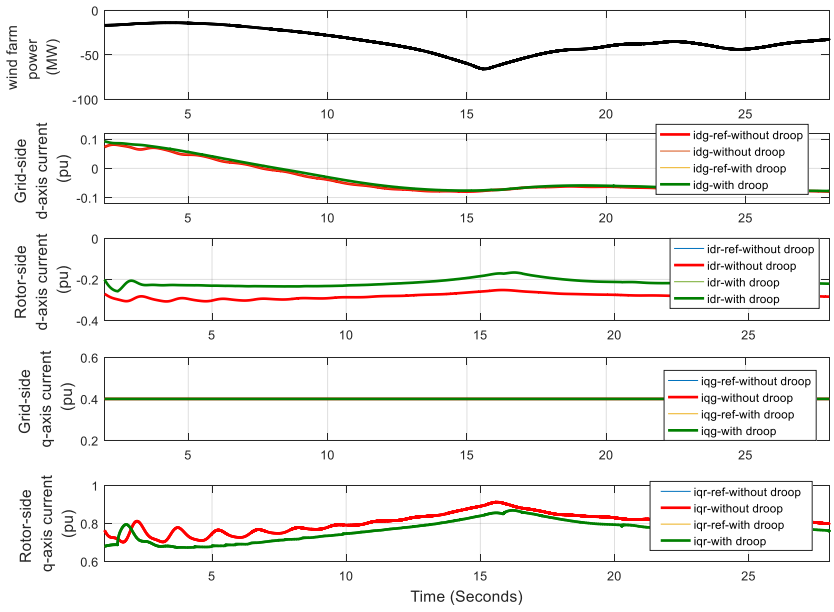

Figure 13. Tracking of inner loop control reference signals in the droop and without droop-fed vector control of the VSPS system along with wind farm.

3.2. Comparison of the Proposed Control Scheme with the Conventional Strategy

3.2.1. Grid Frequency Control and Response

Figure 14a shows the evolution of the network in grid frequency response by comparing the VSPS active power control with and without droop control and the DC-link voltage. While the power

fluctuation of the wind farm occurs in the grid, the VSPS is dedicated to compensate the fluctuations accordingly and smaller deviations in the grid frequency are recorded with droop than without droop control. The waveform of the DC voltage result shows a precise regulated dynamic response and insignificant deviations for wind power fluctuations. The difference in frequency deviations between the two control modes is more significant at a higher wind power fluctuation. It implies that the droop control system is effective for regulating the grid frequency excursions caused by large contingences. Figure 14b shows the evolution of the frequency comparison between these control modes during the start-up transient and when a three-phase fault is imposed at t = 30 s for nine cycles. During the start-up and fault, less excursions in frequency are observed with droop than without droop control. The time taken to dampen the frequency excursions to their nominal value without droop control is much longer than with droop. In this case, the droop control quickly and effectively regulates the frequency dynamics during grid disturbances.

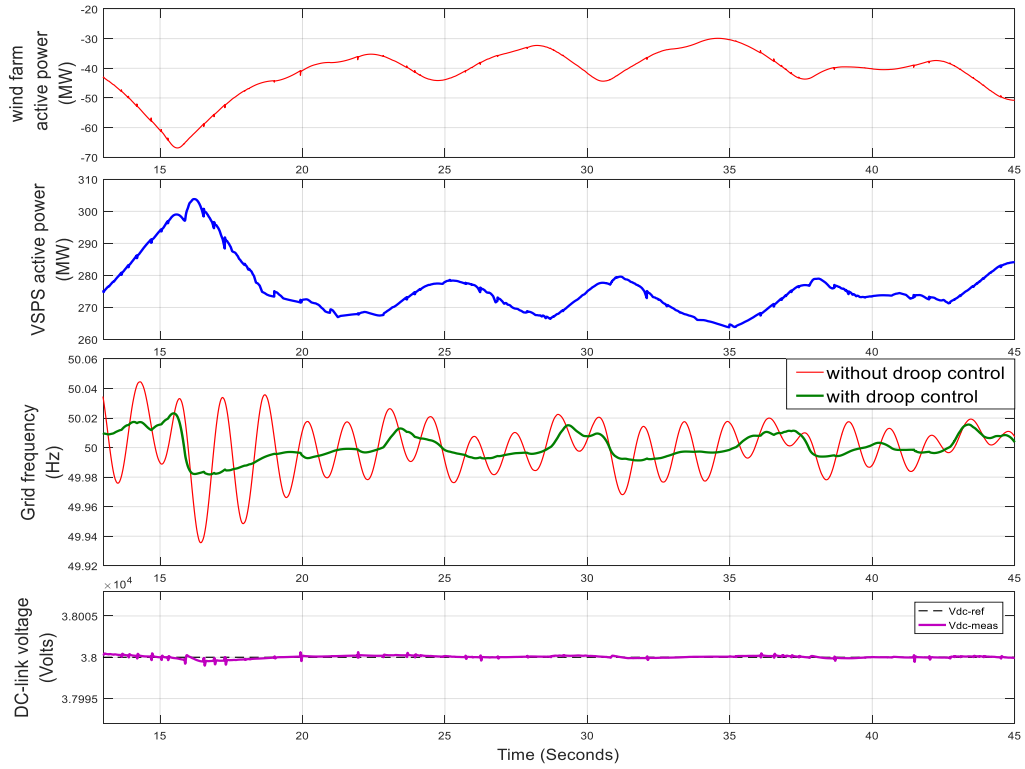

(**a**)

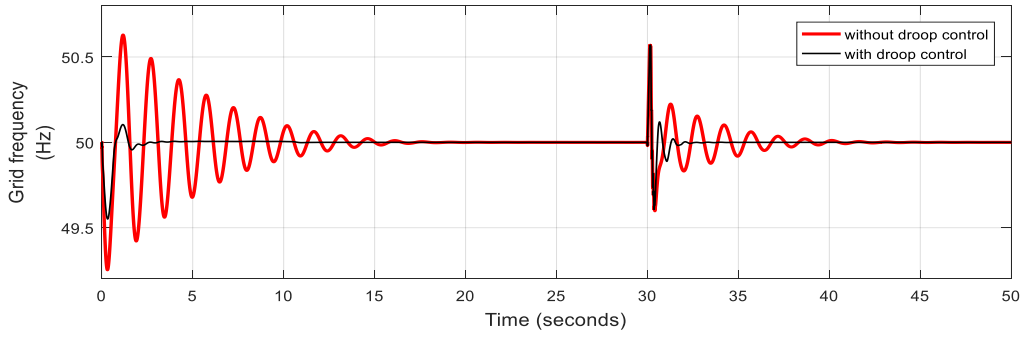

(**b**)

Figure 14. Evolution of the network in grid frequency response comparing the VSPS active power control with and without droop control and the DC link voltage as well: (**a**) while the wind farm power fluctuation exists in the grid; (**b**) during the start-up transient and three phase fault.

3.2.2. AC-Bus Voltage Control and Response

Figure 15 shows the AC-bus voltage regulation and response of the VSPS vector control system with and without being droop-fed. Two cases with different voltage levels are considered; one at the bus terminal of the VSPS plant (B_{vsps}), while the other at bus B_{SG3} in the grid system. In both cases, the AC bus voltage is improved to its nominal value with droop-control than without it. The AC voltage is well regulated as the equivalent reactive power is generated by the induction machine to compensate the voltage droop through the VSC based droop-fed vector control strategy. This verifies the strong known relationship between the reactive power and the AC-bus voltage stated in the load flow equation.

Figure 15 also shows the relationship between wind power fluctuations and AC voltage at buses B_{vsps} and B_{SG3}. When the wind fluctuation is increased, as shown in Figure 15 at t = 15.1 s, there is greater deviation in the AC-bus voltage at both buses in the conventional vector control strategy while it remains the same in the droop-fed control mode. This is because of the direct relationship between the reactive power absorbed from the grid by the induction generator of the wind farm and its active power generation. Therefore, the fluctuation of the active power generation caused by the wind speed variation results in higher absorption of reactive power by the induction generator which leads to AC-bus voltage deviation in the grid. Hence, the VSC based droop control of the VSPS system plays a key role of balancing the generation and absorption of reactive power in the grid at varying active power from the wind farm so as to regulate the AC bus voltage.

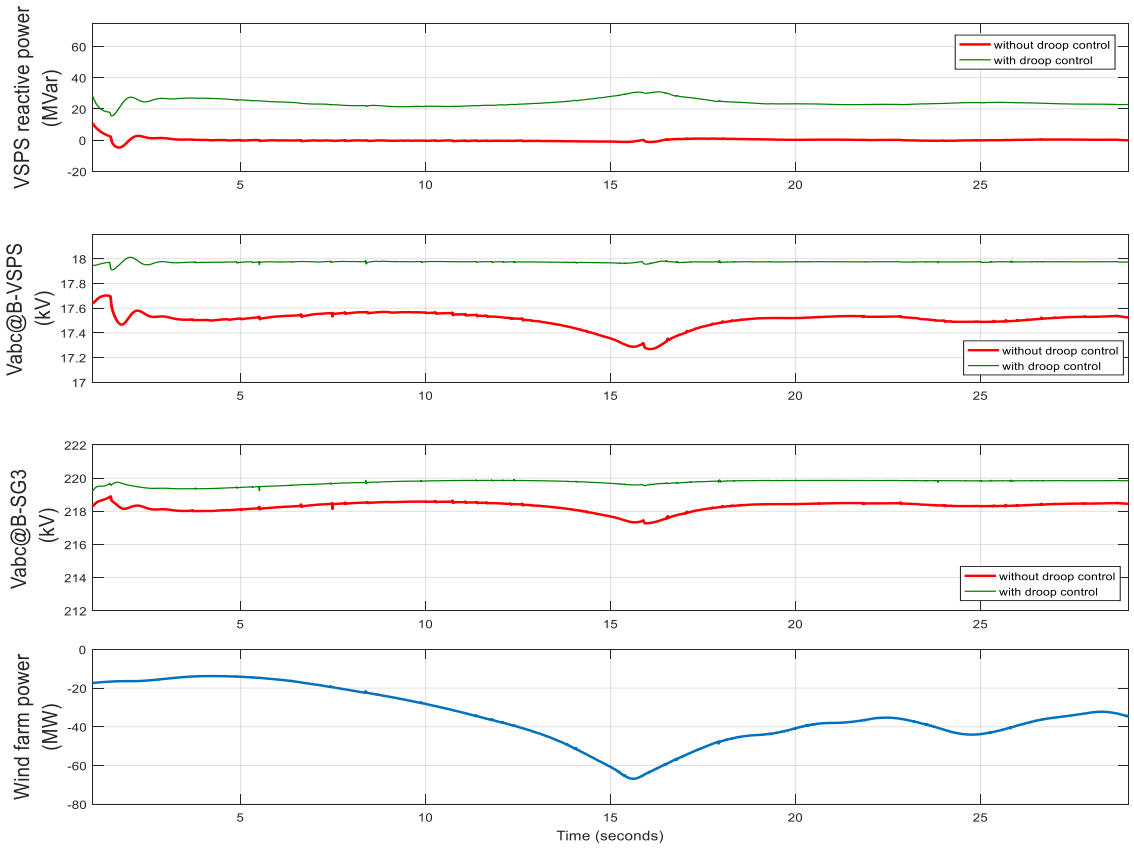

Figure 15. Evolution of the network in AC-bus voltage response of the VSPS control system considered at two buses by comparing the reactive power control with and without droop control while the wind is fluctuating.

3.3. The Frequency and AC Voltage Control and Response During Load Variations

Figure 16 demonstrates the grid frequency and AC bus voltage control and response when 20 MW load is added to the grid at t = 20 s and removed at t = 40 s in order to compare the performances of the

control modes between the droop-feed and without it. In Figure 16a, the evolution is the grid frequency associated with the active power injected at the bus B_{SG3} and the VSPS active power generation while the load is added and removed to and from the grid. The frequency tracks its nominal value very quickly with the droop control than without droop. In the absence of droop control, when the power imbalance occurs, the frequency is very sensitive for deviation and hardly to control timely. The bus power injection is also affected by the frequency fluctuation, but with the droop control, it regulates the power supply/load balance by adjusting the VSPS to increase or decrease its generation accordingly.

Figure 16b simulates the AC bus voltage control associated with the reactive power status of the VSPS plant. When the load is added to the grid, the AC bus voltage decreases more with the control system without droop mode, but in the droop mode, the voltage tracks its nominal value, because of generating more reactive power by the VSPS plant.

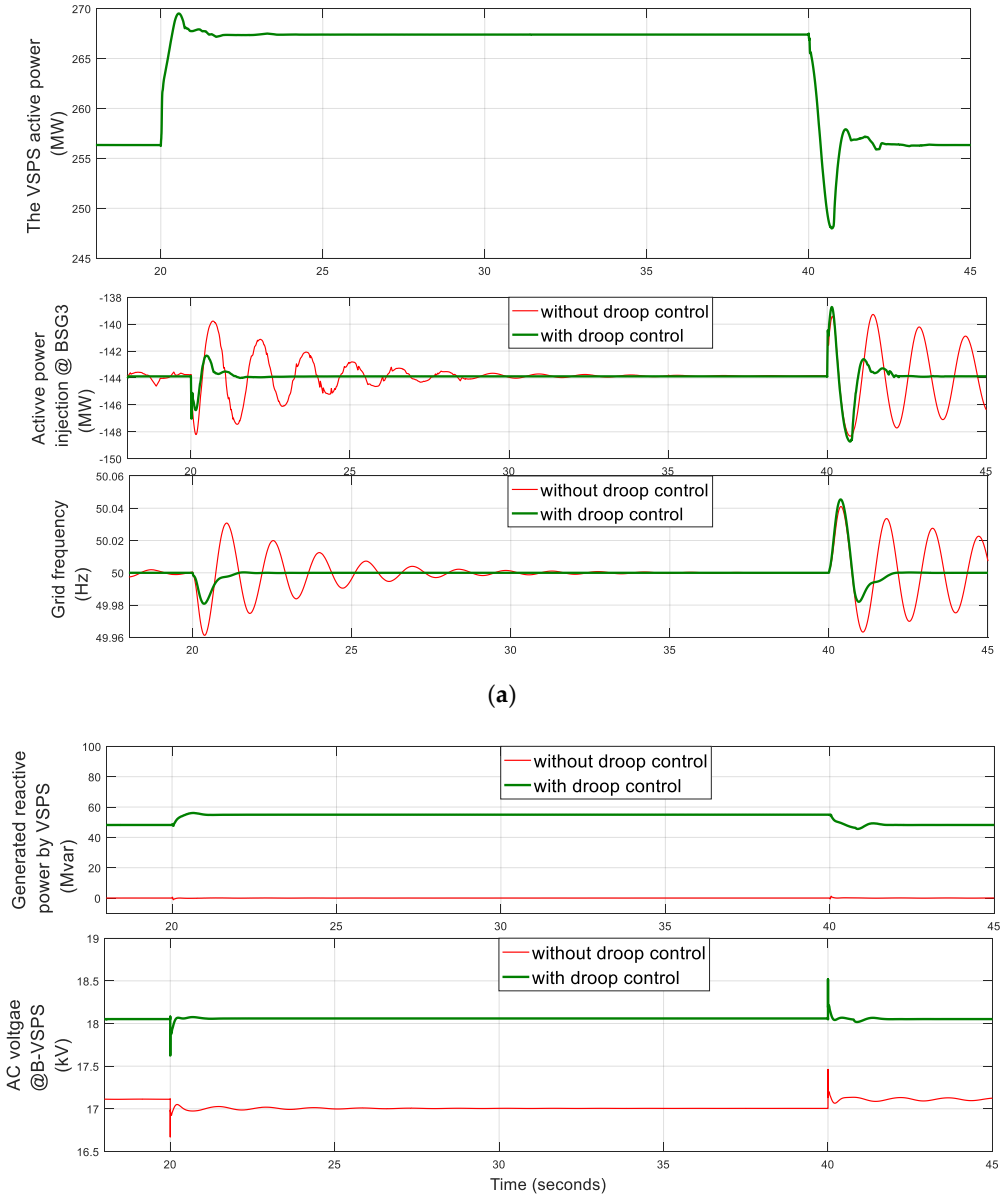

Figure 16. Evolutions of the network in the load variations; (**a**) in frequency control and response associated with active power; (**b**) AC bus voltage control and response associated with reactive power generation by the VSPS.

In general, the droop-fed vector control is quite effective to regulate the grid frequency and AC-bus voltage; in turn, it can help the stability development of the grid which are connected to a renewable energy resources.

4. Conclusions

This paper presents a study on droop-fed vector control strategy-based doubly fed induction machine VSPS system for the reduction of wind power fluctuation impact and other contingencies on grid frequency and AC-bus voltage stability. Mathematical models based on a phasor model technique is presented. A case study of a grid system having five supplies and two loads with seven buses is conducted. The grid includes both synchronous and induction machines. Since the rotor speed rotates synchronously with the rotating magnetic field of the stator of the synchronous machine, the grid frequency is computed from the rotor speed relationship for measuring and estimating to feed the VSPS active power control loop. The performance is validated in a MATLAB/Simulink platform. The results show that the proposed control strategy for the VSPS system achieves better dynamic and steady state controlling responses of grid frequency and AC-bus voltage in the power system than the conventional one while the intermittent wind power, load variations three-phase fault and start-up transients are imposed to the grid with small errors in acceptable ranges in the power grid system.

Author Contributions: Conceptualization, G.T.B. and M.H.; Methodology, G.T.B.; Software, G.T.B.; Validation, G.T.B., M.H. and S.A.M.; Formal Analysis, G.T.B.; Investigation, G.T.B.; Resources, M.H.; Data Curation, G.T.B.; Writing-Original Draft Preparation, G.T.B.; Writing-Review & Editing, M.H., P.S. and S.A.M.; Visualization, G.T.B.; Supervision, M.H.; Project Administration, M.H.; Funding Acquisition, M.H.

Funding: This research received no external funding.

Acknowledgments: This work was supported by the State Key Laboratory of Smart Grid Protection and Control, "111" Project (B08013) of China.

Conflicts of Interest: The authors declare no conflict of interest.

Appendix A

The followings are the main parameters of the system used in this paper:

- A VSC DFIM based VSPS plant; turbine rating = 300 MW; rated hydraulic head=165 m; piping area = 11.15 m^2; gate opening at no load = 0.06 pu and at full load = 0.94 pu; base value is taken as a power of 333 MVA and a voltage of 220 kV
    - power capacity = 333 MVA/18 kV, stator resistance and leakage inductance R_s = 0.0086 pu and L_{ls} = 0.152 pu, rotor resistance and leakage inductance R_r = 0.007 pu and L_{lr} = 0.187 pu, magnetization inductance L_m = 300 pu, inertia constant, friction factor, and pairs of poles H(s) = 10.6, f(pu) = 0.02 and p = 12
    - Converter rating = 66 MVA/38 kV DC voltage, the DC-link equivalent capacitance $C_{eq} = 2 \times 10^{-2}$ Farad, the coupling inductor resistance and inductance R = 0.0025 pu and L = 0.25 pu
    - The rotor side controller Current loop gains (P_i = 1.25 and I_i = 15) Active power loop gains (P_p = 1.5 and I_p = 20) Reactive power loop gains (P_q = 0.3 and I_q = 5.5) Frequency droop constant (K_f = 90) AC voltage droop constant (K_{ac} = 60)
    - The grid side controller Current loop gains (P_{ig} = 1.1 and I_{ig} = 9) DC voltage loop gains (P_{dc} = 0.001 and I_{dc} = 0.02)
    - Grid connecting transformer: capacity = 350 MVA, 18 kV/220 kV, winding parameters $R_1 = R_2$ = 0.0025 pu and $L_1 = L_2$ = 0.08 pu; magnetization resistance and inductance $R_m = L_m$ = 500 pu
- Two hydropower plants (synchronous generator): each has a power capacity = 200 MVA, 13.8 kV; and grid connecting transformer capacity = 350 MVA, 13.8 kV/220 kV.

- A diesel power plant (synchronous generator): Power capacity = 15 MVA, 25 kV; grid connecting transformer capacity = 20 MVA, 25 kV/220 kV.
- A wind farm with induction generator: seven turbines 15 MW capacity each, 575 V; and grid connecting transformer capacity 12 MVA, 575 V/220 kV for each wind turbine
- Load = 630 MVA and the system frequency is 50 Hz.

References

1. Global Wind Energy Council, Global Wind Energy Outlook 2014, October 2014. Available online: https://www.gwec.net/wp-content/uploads/2014/10/GWEO2014_WEB.pdf (accessed on 10 February 2018).
2. International Energy Agency & Energy Research Institute. *China Wind Energy Development Roadmap 2050*; International Energy Agency & Energy Research Institute: Paris, France, 2011.
3. Li, W.; Joós, G.; Abbey, C. Wind power impact on system frequency deviation and an ess based power filtering algorithm solution. In Proceedings of the 2006 IEEE PES Power Systems Conference and Exposition, 29 October–1 November 2006; pp. 2077–2084.
4. Chowdhury, M.A.; Hosseinzadeh, N.; Shen, W.X. Smoothing wind power fluctuations by fuzzy logic pitch angle controller. *Renew. Energy* **2012**, *38*, 224–233. [CrossRef]
5. Song, X.; Bitew, G.T.; Han, M.; Meng, Z.; Xu, J.; Wang, X. Stability and control of a grid integrated dfim based variable speed pumped storage system. In Proceedings of the 2017 International Electrical and Energy Conference (CIEEC 2017), Beijing, China, 25–27 October 2017; pp. 175–181.
6. Bocquel, A.; Janning, J. Analysis of a 300 MW variable speed drive for pump-storage plant applications. In Proceedings of the 2005 European Conference on Power Electronics and Applications, Dresden, Germany, 11–14 September 2005; pp. 1–10.
7. Furuya, S.; Taguchi, T.; Kusunoki, K.; Yanagisawa, T.; Kageyama, T.; Kanai, T. Successful achievement in a variable speed pumped storage power system at Yagisawa power plant. In Proceedings of the Conference Record of the Power Conversion Conference—Yokohama 1993, Yokohama, Japan, 19–21 April 1993; pp. 603–608.
8. Chang, X.; Han, M.; Zheng, C. Power control analysis for variable speed pumped storage with full-size converter. In Proceedings of the IECON 2015—41st Annual Conference of the IEEE Industrial Electronics Society, Yokohama, Japan, 9–12 November 2015; pp. 001327–001332.
9. Abdalla, O.H.; Han, M.; Liu, C. Multi-level converter based variable speed pump storage for wind power compensation. In Proceedings of the 2014 International Conference on Information Science, Electronics and Electrical Engineering, Sapporo, Japan, 26–28 April 2014; pp. 1497–1501.
10. Steimer, P.K.; Senturk, O.; Aubert, S.; Linder, S. Converter-fed synchronous machine for pumped hydro storage plants. In Proceedings of the 2014 IEEE Energy Conversion Congress and Exposition (ECCE), Pittsburgh, PA, USA, 14–18 September 2014; pp. 4561–4567.
11. Pronin, M.V.; Shonin, O.B.; Vorontsov, A.G.; Gogolev, G.A. Features of a drive system for pump-storage plant applications based on the use of double-fed induction machine with a multistage-multilevel frequency converter. In Proceedings of the 2012 15th International Power Electronics and Motion Control Conference (EPE/PEMC), Novi Sad, Serbia, 4–6 September 2012; pp. DS1b.7-1–DS1b.7-8.
12. Xu, L.; Cartwright, P. Direct active and reactive power control of dfig for wind energy generation. *IEEE Trans. Energy Convers.* **2006**, *21*, 750–758. [CrossRef]
13. Bourdoulis, M.K.; Alexandridis, A.T. Direct power control of dfig wind systems based on nonlinear modeling and analysis. *IEEE J. Emerg. Sel. Top. Power Electron.* **2014**, *2*, 764–775. [CrossRef]
14. Datta, R.; Ranganathan, V.T. Direct power control of grid-connected wound rotor induction machine without rotor position sensors. *IEEE Trans. Power Electron.* **2001**, *16*, 390–399. [CrossRef]
15. Bitew, G.T.; Han, M.; Simiyu, P.; Zmarrak, W.K.; Luu, K.T.; Faisal, M.S. Direct power control strategy based variable speed pumped storage system for the reduction of the wind power fluctuation impact on the grid stability. In Proceedings of the 12th IEEE International Conference on Compatibility, Power Electronics, and Power Engineering, Doha, Qatar, 10–12 April 2018.
16. Merzoug, M.; Naceri, F. Comparison of field-oriented control and direct torque control for Permanent Magnet Synchronous Motor (PMSM). *Int. J. Electr. Comput. Energ. Electron. Commun. Eng.* **2008**, *2*, 1796–1802.
17. Kundur, P. *Power System Stability and Control*; McGraw-Hill, Inc.: New York, NY, USA, 1994.

18. Maghamizadeh, M.; Fathi, S.H. Virtual flux based direct power control of a three-phase rectifier connected to an lcl filter with sensorless active damping. In Proceedings of the 2016 7th Power Electronics and Drive Systems Technologies Conference (PEDSTC), Tehran, Iran, 16–18 February 2016; pp. 476–481.
19. Djeriri, Y.; Meroufel, A.; Massoum, A.; Boudjema, Z. A comparative study between field oriented control strategy and direct power control strategy for DFIG. *J. Electr. Eng.* **2014**, *14*, 169–178.
20. Johar, M.; Radan, A.; Miveh, M.R.; Mirsaeidi, S. Comparison of dfig and synchronous machine for storage hydro-power generation. *Int. J. Pure Appl. Sci. Technol.* **2011**, *7*, 48–58.
21. MATLAB Package Center. Available online: https://www.mathworks.com/ (accessed on 1 May 2018).
22. Gihga, R.; Wu, Q.; Nielsen, A.H. Phasor model of full scale converter wind turbine for small-signal stability analysis. *J. Eng.* **2017**, *2017*, 978–983. [CrossRef]
23. Bitew, G.T.; Han, M.; Meng, Z.; Song, X.; Xu, J.; Simiyu, P. Phasor model simulation of a grid integrated variable speed pumped storage system. *J. Eng.* **2017**, *2017*, 1002–1009.
24. Haileselassie, T.M.; Uhlen, K. Primary frequency control of remote grids connected by multi-terminal HVDC. In Proceedings of the IEEE PES General Meeting, Providence, RI, USA, 25–29 July 2010; pp. 1–6.
25. Vector Control. Available online: https://en.wikipedia.org/wiki/Vector_control/ (accessed on 3 May 2018).
26. Noguchi, T.; Tomiki, H.; Kondo, S.; Takahashi, I. Direct power control of pwm converter without power-source voltage sensors. *IEEE Trans. Ind. Appl.* **1998**, *34*, 473–479. [CrossRef]
27. Du, C.; Agneholm, E.; Olsson, G. Use of vsc-hvdc for industrial systems having onsite generation with frequency control. *IEEE Trans. Power Deliv.* **2008**, *23*, 2233–2240. [CrossRef]
28. Azbe, V.; Mihalic, R. Transient stability of doubly-fed induction machine in parallel to synchronous machine. In Proceedings of the 2015 IEEE Eindhoven PowerTech, Eindhoven, The Netherlands, 29 June–2 July 2015; pp. 1–6.
29. Yazdani, A.; Iravani, R. *Voltage-Sourced Converters in Power Systems; Modeling, Control, and Applications*; John Wiley & Sons, Inc.: Hoboken, NJ, USA, 2010.
30. Demiray, T.; Andersson, G.; Busarello, L. Evaluation study for the simulation of power system transients using dynamic phasor models. In Proceedings of the 2008 IEEE/PES Transmission and Distribution Conference and Exposition: Latin America, Bogota, Colombia, 13–15 August 2008; pp. 1–6.